Bioconjugate Chemistry

Article

pubs.acs.org/bc

Bimodal Imaging of Inflammation with SPECT/CT and MRI Using Iodine-125 Labeled VCAM-1 Targeting Microparticle Conjugates

N. Patel,[†,‡,#] B. A. Duffy,[†,#] A. Badar,[†] M. F. Lythgoe,[†] and E. Årstad*[,‡]

[†]Centre for Advanced Biomedical Imaging (CABI) and [‡]Division of Medicine and Department of Chemistry and Institute of Nuclear Medicine, University College London, London NW1 2BU, United Kingdom

Supporting Information

ABSTRACT: Upregulation of cell adhesion molecules on endothelial cells is a hallmark of inflammation and an early feature of several neurological conditions. Here, we describe bimodal *in vivo* imaging of this inflammatory event in the brain using functionalized micron-sized particles of iron oxide. The particles were conjugated to anti-VCAM-1 antibodies and subsequently labeled with iodine-125. Radiolabeling of the antibody-coated particles was straightforward and proceeded in high radiochemical yields using commercially available iodination tubes. The corresponding contrast agent was evaluated in a rat model of cerebral inflammation based on intracerebral injection of tumor necrosis factor alpha and a rat model of status epilepticus. Biodistribution studies and phosphorimaging of cryosections were used to verify *in vivo* imaging data obtained with single photon emission computed tomography (SPECT) and magnetic resonance imaging (MRI). The contrast agent showed rapid and highly localized binding to the vasculature of inflamed brain tissue, and was effectively cleared from the blood pool within 2 min postinjection. Overall, the pattern of hypointensities observed with MRI was in good agreement with the distribution of the contrast agent as determined with SPECT and phosphorimaging; however, conspicuous differences in the signal intensities were observed. The results demonstrate that radiolabeled micron-sized particles of iron oxide enable multimodal *in vivo* imaging with MRI and nuclear techniques, and highlight the value of validating different imaging methods against one another.

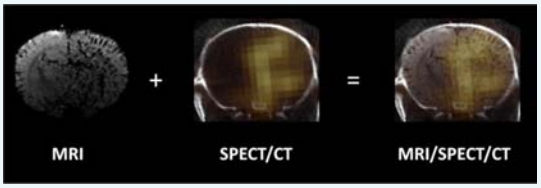

INTRODUCTION

Cerebral inflammation occurs as a result of infection or injury and is known to be a feature of several neurological conditions such as stroke,[1] epilepsy,[2] traumatic brain injury,[3] brain tumors,[4,5] and Alzheimer's disease.[6] Molecular imaging is a powerful tool which could help to determine which inflammatory processes are beneficial and which may be detrimental to patient outcome. Furthermore, it could be used for anti-inflammatory treatment monitoring and to identify which patients might benefit from such therapies.

Recently, imaging vascular cell adhesion molecule-1 (VCAM-1) expression using micron-sized particles of iron oxide (MPIOs) coupled with magnetic resonance imaging (MRI) has shown to be a highly sensitive and specific method of detecting and locating inflammation.[7−14] The low constitutive expression of VCAM-1 renders it an ideal target for molecular imaging. It is expressed on the surface of endothelial cells and therefore can be used to monitor pathology or therapies in the brain without the need for contrast agents to cross the blood-brain barrier (BBB). VCAM-1 mediates the rolling and extravasation of leukocytes across the vascular endothelium.[15] Furthermore, it is thought to play a key role in several pathological conditions and may therefore provide a meaningful biomarker of disease progression. For example, it has been suggested that VCAM-1 can be hijacked by tumor cells to aid adhesion to the vascular endothelium[4] and may exacerbate the initiation of seizures (ictogenesis) or the development of epilepsy (epileptogenesis).[16]

The development of anti-VCAM-1 antibody coated MPIOs as contrast agents (CAs) for MRI has been a major technological advance as it enables neuroinflammation to be detected and localized with high sensitivity and specificity.[7,10] This has challenged the notion that MRI has insufficient sensitivity for molecular imaging in the brain, a domain traditionally restricted to nuclear imaging modalities. MPIOs provide marked contrast on MRI images, which can be attributed to the sizable payload of iron which in turn results in hypointense regions up to 50 times the physical diameter of the particles.[17] However, particle size also affects the cellular interactions, distribution, and clearance of CAs.

The exquisite performance of MPIOs as CAs for MRI is intriguing as extensive efforts over the past decade to develop particle-derived nuclear imaging agents has met with limited success, despite the superior detection limits of positron emission tomography (PET) and single photon emission computed tomography (SPECT).[18−21] In order to gain further insights into their properties as CAs, we have labeled VCAM-1 antibody coated MPIOs with iodine-125 (half-life 60 days). The presence of radioactive iodine enables *ex vivo* biodis-

Received: March 31, 2015
Revised: July 27, 2015
Published: July 28, 2015

DOI: 10.1021/acs.bioconjchem.5b00380
Bioconjugate Chem. 2015, 26, 1542−1549

tribution studies, measurement of blood clearance, and validation of the observed MRI contrast with *in vivo* nuclear imaging and *ex vivo* phosphorimaging. A further motivation for this work was to determine whether MPIOs can be exploited as radiotracers for biomodal imaging of molecular targets in the vasculature. Herein, we report SPECT and MR imaging of inflammation in a TNF-α model, and in the lithium–pilocarpine model of Status Epilepticus (SE).

RESULTS

Radiochemistry. The radiolabeled contrast agent was obtained directly from antibody coated MPIOs by incubation with [^{125}I]NaI in precoated iodogen tubes, and was isolated by magnetic immobilization to give [^{125}I]VCAM-MPIO in 85 ± 5% (n = 11) radiochemical yield. Iodine-125 was used due to the ease of labeling, long half-life (60 days), and low energy gamma emission (maximum energy 35 keV), which allowed *in vivo* imaging data to be corroborated by *ex vivo* phosphorimaging of brain sections.

Biodistribution Studies. In healthy rats, [^{125}I]VCAM-MPIO displayed rapid kinetics and was effectively cleared from the blood pool 2 min post-injection (Figure 1a). Within 10 min, the CA accumulated in the lungs (4.8 ± 1.3%ID/g), spleen (3.4 ± 1.4%ID/g) and liver (1.5 ± 0.5%ID/g), with negligible uptake in the brain (0.016 ± 0.005%ID/g) (Figure 1b and Supporting Information Table 1). The low radioactivity levels in the bladder and thyroid, as seen by whole body SPECT/CT 20–25 min post-injection (Figure 1c), suggest that [^{125}I]VCAM-MPIO remains largely intact after administration *in vivo*. The discrepancies between the measured tissue distribution of the contrast agent at 10 min p.i. and the whole body SPECT image (20–25 min p.i.), can at least in part be explained by the low density of lung tissue and the different units of quantification; whereas organ distribution is normalized to weight, SPECT provides a measure of radioactivity levels per volume. However, the results may also reflect clearance from the lungs to the liver and spleen over time.

Dose Optimization Studies in the TNF-α Induced Model of Neuroinflammation. To allow sequential imaging with SPECT/CT and MRI in individual animals, dose optimization studies were performed in rats that were injected with TNF-α in the right striatum to induce inflammation. Following an initial study, 2 mg Fe/kg of [^{125}I]VCAM-MPIO appeared to be insufficient to give discernible hypointensities with MRI (Figure 2a). Hence, we used increasing doses of VCAM-MPIO to determine a suitable concentration range for MRI (Figure 2b,c). As expected, the MRI contrast effect appeared dependent on the amount VCAM-MPIO administered, and was only apparent at the higher doses. At 5 mg Fe/kg, there was a pronounced difference between TNF-α treated animals, animals treated with saline, and TNF-α treated animals that received the nonspecific CA (IgG-MPIO). As previously reported,[10] limited hypointense regions were observed in the brains of animals from the two control groups (Figure 2d and e). At the selected concentration of VCAM-MPIO (5 mg Fe/kg), imaging with SPECT/CT showed localized binding of the CA in the brains of TNF-α treated animals, consistent with neuroinflammation, when using two different radioactivity levels (0.25 and 0.90 MBq per gram of body weight) (Figure 2f and g). As judged by the relative intensities of signals in the brain and the extracranial regions, radioactivity levels of approximately 0.25 MBq per gram of body weight appeared optimal (Figure 2f), whereas a higher dose (0.90 MBq per gram of body weight) resulted in a disproportionate increase in background noise (Figure 2g). No brain uptake was observed in the saline control group at either dose level (Figure 2h and i). Five milligrams Fe/kg was sufficient for segmentation of hypointense regions (Figure 2j–l). In the TNF-α group, dynamic imaging with SPECT using 5 min frames from 20 to 45 min post-injection revealed that the binding of [^{125}I]VCAM-MPIO to the brain vasculature remained largely unchanged over this period of time (SI Figure 1). For this reason, we adopted a protocol with SPECT/CT commencing at 20 min after administration of the CA, followed by imaging with MRI 45 min later, and subsequently, brains were extracted for *ex vivo* phosphorimaging.

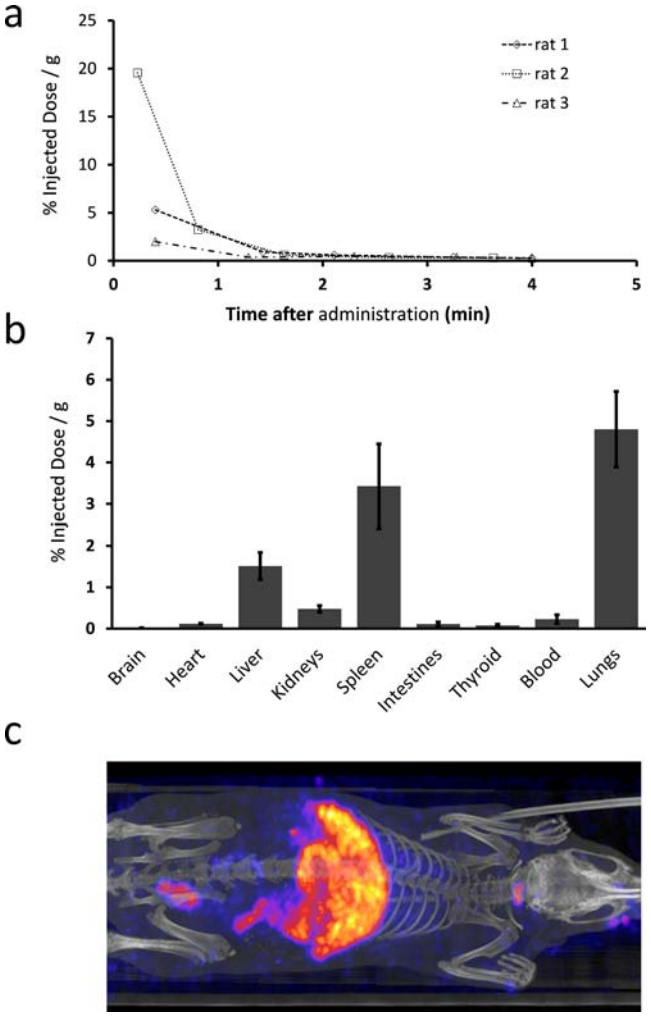

Figure 1. (a) Blood clearance and (b) biodistribution of ^{125}I-labeled VCAM-MPIO in healthy rats. For biodistribution studies, the animals were euthanized 10 min post tracer administration and the results are displayed as %ID/g (n = 3) ± SEM. (c) Whole body SPECT/CT maximum intensity projection 20 min post CA administration (5 mg Fe/kg, 0.25 MBq/g per gram, n = 1).

Qualitative Comparison of MRI, SPECT/CT, and Phosphorimaging. To facilitate comparison of the data, the MRI images were overlaid on the SPECT/CT images (Figure 3a–d). In TNF-α treated rats (n = 4), the hypointensities present on MRI were in good agreement with the SPECT signals in the brain, and also correlated well with phosphorimaging of cryosections from the site of TNF-α injection (Figure 3f–h). However, the distribution of [^{125}I]VCAM-

DOI: 10.1021/acs.bioconjchem.5b00380
Bioconjugate Chem. 2015, 26, 1542–1549

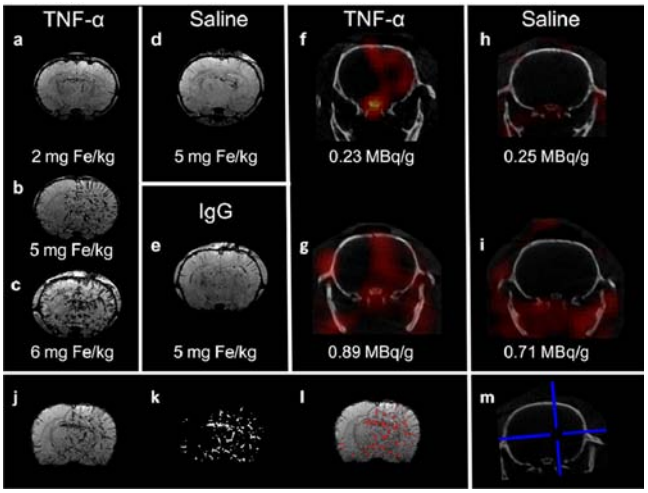

Figure 2. Representative coronal MRI and SPECT images demonstrating binding of radiolabeled VCAM-MPIO at different doses of contrast agent (a–c) and levels of radioactivity (f–i). (a–c) TNF-α group following administration of VCAM-MPIO: (a) 2 mg Fe/kg, (b) 5 mg Fe/kg, and (c) 6 mg Fe/kg. The optimum dose of iron oxide (5 mg Fe/kg) was assessed in two control groups: (d) saline and (e) IgG. (f–i) SPECT/CT in the TNF-α and saline groups administered with a lower and higher dose of radioactivity: (f) TNF-α (0.25 MBq/g), (g) TNF-α (0.90 MBq/g), (h) Saline (0.25 MBq/g), (i) Saline (0.71 MBq/g). (j–l) Illustration of quantification procedure: (j) brain extraction, (k) hypointense regions are segmented using local thresholding, (l) segmented regions overlaid in red upon the original MRI image, (m) blue crosshairs indicate the approximate location of the coronal slices for the displayed MRI and SPECT/CT images. For display purposes, SPECT images are thresholded at 40% of the 95th percentile and linearly scaled between this value and the 95th percentile.

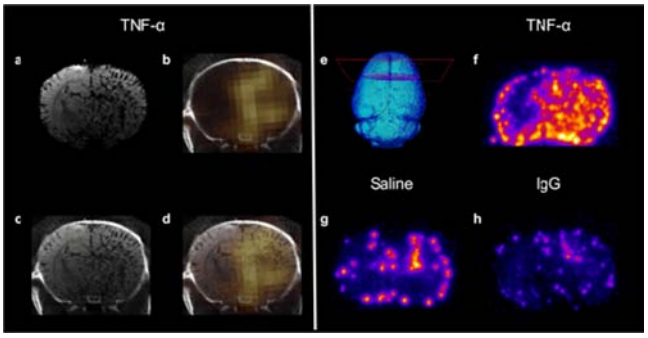

Figure 3. Bimodal *in vivo* imaging and *ex vivo* phosphorimaging of VCAM-1 expression. (a–d) Intracerebral TNF-α + [^{125}I]VCAM-MPIO (5 mg Fe/kg): (a) coronal MRI image, (b) coronal SPECT/CT image, (c) co-registered MRI and CT image, (d) SPECT overlaid on MRI image. (e) Illustration of the approximate location for coronal sections. (f–h) Coronal phosphorimaging sections: (f) TNF-α, (g) saline control, (h) IgG control.

MPIO in the cryosections appeared more widespread than was evident from the *in vivo* imaging data obtained with MRI and SPECT. Interestingly, in the saline treated control group, phosphorimaging showed localized uptake of the CA at the injection site, suggesting that the sham treatment also induced local inflammation (Figure 3g). The low and homogeneous radioactivity levels observed with phosphorimaging in brains from animals that received [^{125}I]IgG-MPIO confirms that the nonspecific binding of the CA is negligible (Figure 3h).

Quantitative Comparison of SPECT and MRI Data. To enable quantitative comparison of the data obtained with SPECT/CT and MRI, we determined the total signal from [^{125}I]VCAM-MPIO in the whole brain, as well as in the two hemispheres. In the case of MRI, this was expressed as the percentage contrast void across the brain volume. For SPECT, the background was defined as the average mean signal intensity across the extracranial field of view, and uptake of the CA was expressed as the signal-to-background ratio in order to normalize counts for body weight and the amount of radioactivity that was administered. Importantly, injection of TNF-α into the right striatum induces widespread inflammation that also affects the left hemisphere, as can be seen by 3D representation of MRI images (Figure 4a,b). Nevertheless, comparison of the signal in the two brain hemispheres avoids

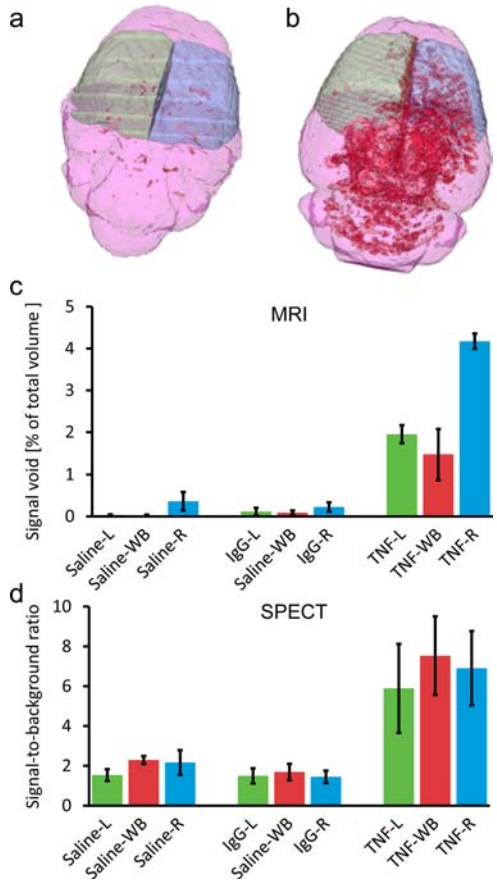

Figure 4. 3D representation of CA binding and *in vivo* quantitation using SPECT and MRI. 3D representation of CA binding (VCAM-MPIO, 5 mg Fe/kg) based on *in vivo* MRI images for the (a) saline control group and the (b) TNF-α treated group. Segmented hypointense regions are shown in red, while the pink, green, and blue areas indicate the whole brain, left, and right regions of interest (respectively) used for quantification. Quantification of VCAM-MPIO binding as assessed by (a) *in vivo* MRI and (b) *in vivo* SPECT. Quantification was carried out over the whole brain (red) as well as the left (green) and right (blue) cerebral hemispheres. The saline group received intracerebral saline injections followed by radiolabeled VCAM-MPIO (5 mg Fe/kg, 0.25–0.9 MBq/g) (n = 3). The IgG group received intracerebral TNF-α injections followed by radiolabeled IgG-MPIO (5 mg Fe/kg, 0.25–0.9 MBq/g) (n = 3) and the TNF-α group received intracerebral TNF-α injections followed by radiolabeled VCAM-MPIO (5 mg Fe/kg, 0.25–0.9 MBq/g) (n = 4). Abbreviations: L—Left, WB—Whole brain, R—Right.

DOI: 10.1021/acs.bioconjchem.5b00380
Bioconjugate Chem. 2015, 26, 1542–1549

bias from manually defining the regions of interest, and was used in order to highlight differences in the data obtained with MRI and SPECT. Quantitation with both MRI and SPECT revealed higher CA binding in TNF-α treated animals as compared to the two control groups, globally as well as in each of the brain hemispheres (Figure 4c,d and SI Figure 2). In the TNF-α treated animals, [^{125}I]VCAM-MPIO localized predominantly to the affected (right) cerebral hemisphere (n = 4) as assessed by both SPECT (p = 0.03) and MRI (p = 0.002). While the SPECT and MRI data were in good overall agreement, there are important differences in the results obtained with the two modalities. In particular, MRI analysis indicated more pronounced difference in CA uptake between the left and right hemispheres in the TNF-α group than was evident with SPECT, and the statistical significance for the group comparisons with MRI was substantially higher than for SPECT. For instance, the difference in the group means when comparing CA uptake in the right hemisphere reached a significance of $p = 1 \times 10^{-6}$ with MRI, but only p = 0.045 with SPECT (Figure 4c,d). Unfortunately, the radioactivity levels that were needed for imaging with SPECT/CT were too high to allow quantification of the CA in brain sections with phosphorimaging.

Distribution of [^{125}I]VCAM-MPIO within the Brain Vasculature. To determine the distribution of [^{125}I]VCAM-MPIO within the brain vasculature, one TNF-α treated rat was administered a reduced dose of [^{125}I]VCAM-MPIO (3 mg Fe/kg, 30 KBq/g). Phosphorimaging of brain cryosections (1 h time point, Figure 5) revealed the CA to be distributed in a

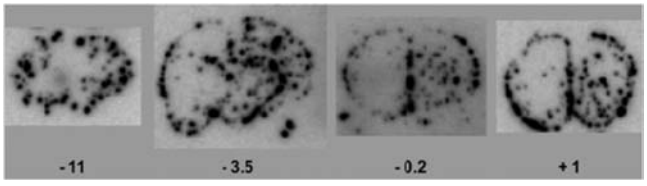

Figure 5. Phosphorimages of coronal brain sections (20 μm) from a TNF-α treated animal administered [^{125}I]VCAM-MPIO (3 mg/kg, 30 kBq/g). The distances of the brain sections shown from the bregma are indicated in mm.

pattern consistent with the hypointensities observed with MRI (SI Figure 3) on slices both anterior and posterior to bregma. While the iron oxide particles appear to be localized in the vasculature, it is unclear whether they are on the arterial or venous side of the circulation. Nevertheless, several large vessels consistent with major arteries were identified: these include the anterior striate arteries (astr), anterior choroidal artery (ach), transverse hippocampal arteries (trhi), the supracollicular network (scol),[22] as well as the choroidal artery. The prominent vessels which lie on the dorsal surface of both hemispheres also contained high levels of the CA.

Imaging of Inflammation in the Lithium−Pilocarpine Model of Status Epilepticus. We also assessed the potential of [^{125}I]VCAM-MPIO as a bimodal imaging agent to detect inflammation in the lithium−pilocarpine model of Status Epilepticus (SE). All pilocarpine treated animals progressed to SE and displayed akinesia and facial automatizms. Tonic−clonic seizures and SE were induced 40−50 min after pilocarpine administration. The seizures were terminated after 90 min by administration of diazepam (10 mg/kg). Approximately 20 h after induction of SE, [^{125}I]VCAM-MPIO (5 mg Fe/kg, 0.25 MBq/g) was administered and the animals were imaged at the optimal time point as identified in the study with TNF-α treated rats (vide supra). With SPECT/CT (SE_{VCAM} group, n = 3), highly localized uptake of the CA was apparent in the cerebellum, cortex, brain stem, and olfactory bulb (Figure 6a−c). With MRI, hypointensities were

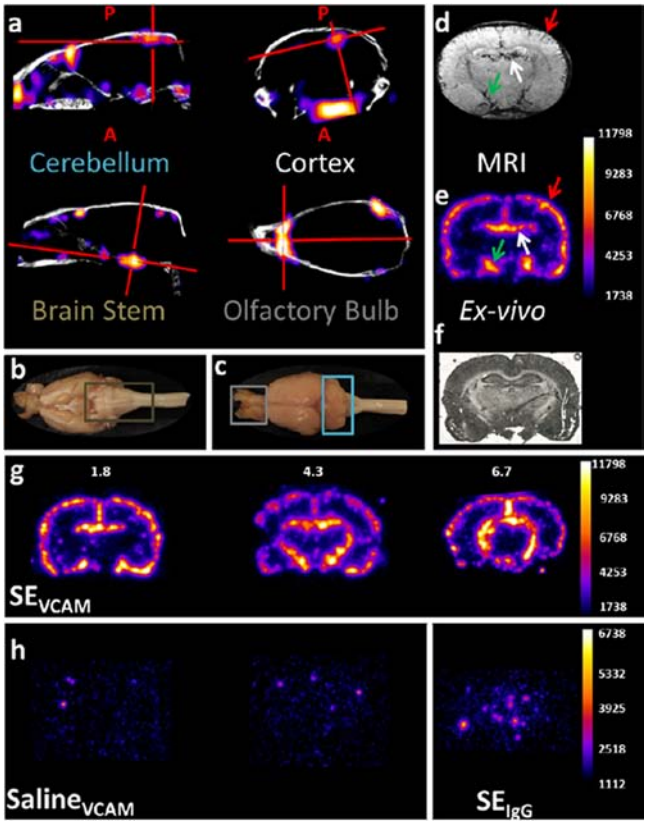

Figure 6. (a) Representative SPECT/CT images from a rat administered [^{125}I]VCAM-MPIO (5 mg Fe/kg, 0.25 MBq/g) approximately 20 h after SE onset. Strong binding can be seen in the cerebellum, cortex, brain stem, and olfactory bulb as viewed in the sagittal (cerebellum and brain stem), coronal (cortex), and transversal (olfactory bulb) slices. The (b) brain stem, (c) cerebellum, and olfactory bulb are highlighted on an optical image of the rat brain. High uptake of the CA was also observed with MRI (d) and phosphorimaging (e) near the hippocampus and subfornical organ (white arrows), as well as at the cortex (red arrows) and hypothalamus (green arrows). (f) Optical image of the brain section shown in (e); P = Posterior, A = anterior from the injection site. (g and h) Phosphorimages of coronal brain sections (40 μm) from the (g) SE_{VCAM} group ([^{125}I]VCAM-MPIO: 5 mg Fe/kg, 0.25 MBq/g); (h) $Saline_{VCAM}$ ([^{125}I]VCAM-MPIO: 5 mg Fe/kg, 0.07 MBg/g) and SE_{IgG} ([^{125}I]IgG-MPIO: 5 mg/kg, 0.07 MBq/g). For the SE_{vcam} group, the approximate locations of the sections displayed are given in mm. The thresholding of the phosphorimages has been adjusted to account for the amount of radioactivity administered.

mainly observed near the hippocampus and ventricles, but also in the cerebral cortex and hypothalamic regions (Figure 6d). Phosphorimaging of coronal brain cryosections confirmed high uptake of [^{125}I]VCAM-MPIO in the cortex, hippocampus, and hypothalamus (Figure 6e−g). As seen for the TNF-α treated animals, [^{125}I]VCAM-MPIO distributed predominantly to larger blood vessels in the SE_{VCAM} group. In the slices proximal to the lambda, uptake of the CA was dominant at the choroid plexus and within the vasculature, in particular in the middle

DOI: 10.1021/acs.bioconjchem.5b00380
Bioconjugate Chem. 2015, 26, 1542−1549

cerebral artery (Figure 6g). No uptake of the CA was evident in brains from sham treated animals ($SALINE_{VCAM}$, $n = 3$), nor in control animals that received [^{125}I]IgG-MPIO (SE_{IgG} group, $n = 3$) (Figure 6h).

DISCUSSION

We have used iodine-125 labeled, VCAM-1 antibody coated, micron-sized particles of iron oxide in two models of neuroinflammation and have shown, for the first time, its potential as a bimodal imaging agent; conspicuity of the CA was not only evident by MRI, but also seen with SPECT/CT and phosphorimaging. Our kinetic studies revealed that [^{125}I]VCAM-MPIO binds rapidly to vasculature in inflamed brain tissue and is quickly cleared from the blood pool. The blood clearance rate of [^{125}I]VCAM-MPIO was in good agreement with previously reported data for other microsized particles.[23] This is significant, as the rapid binding and clearance makes microsized particles suitable for labeling with short-lived positron emitters, such as gallium-68 and fluorine-18, for imaging of molecular targets in the vasculature with PET. It is noteworthy that previous efforts to develop particle-derived radiotracers to date have focused almost exclusively on nanoparticles,[18−21] despite the need for exotic long-lived radionuclides, such as copper-64 (half-life 12.7 h) and iodine-124 (half-life 4.2 days), to match the prolonged circulation time in the blood.[24]

Overall, there was good colocalization between the *in vivo* SPECT and MRI images, and significantly more contrast agent was detected with both imaging techniques in rats treated with TNF-α compared to the two control groups. However, quantification of the imaging data yielded marked differences between the two techniques. This may, at least in part, be explained by attenuation of the low energy γ rays emitted by iodine-125 (35 keV) that was used for SPECT. In addition, the nonlinear relationship between the local CA concentration and contrast volume as assessed by MRI[25] may have further exacerbated the discrepancies in quantification.

In the SE model, SPECT and MRI provided highly complementary data with MRI hypointensities observed around the hippocampus, the subfornical organ, and to a lesser extent in the cerebral cortex. In contrast, SPECT/CT failed to detect the binding of [^{125}I]VCAM-MPIO in the hippocampus (Figure 6), likely due to attenuation, but revealed highly localized signals in the cortex, cerebellum, brain stem, and olfactory bulb (Figure 6a−d). Although the MRI data largely reflected the distribution of [^{125}I]VCAM-MPIO within the brain of SE animals, comparison with SPECT and phosphorimaging highlight the limitations of the MRI contrast effect for imaging in the outer regions of the brain. It is also evident that the relationship between the volume of hypointense pixels within the brain and the concentration of [^{125}I]VCAM-MPIO is nonlinear, which should be taken into account when using this agent.

It is unclear to which degree the distribution of the CA is dependent on cerebral blood flow. Phosphorimaging of brain sections showed that the CA localizes to large blood vessels, which may imply a flow component (Figure 5a). Although the distribution to the larger vessels may be the result of a significant first pass extraction, further studies are required to determine how the interplay between blood flow, extraction, and VCAM-1 expression affects the binding of VCAM-MPIO. While it was outside the scope of this study to investigate the pathology of the disease models in detail, it is worth noting that the distribution pattern of [^{125}I]VCAM-MPIO in the brains of animals from the SE model was consistent with our previously reported results,[10] and demonstrates that the uptake reflects the regions associated with inflammation.

In conclusion, we have developed a highly efficient and practical method to label VCAM-1 antibody coated iron oxide microsized particles with iodine-125, and characterized the contrast agent in two models of inflammation using SPECT/CT, MRI, and phosphorimaging. Kinetic studies showed that binding of [^{125}I]VCAM-MPIO to the vasculature of inflamed tissue remained relatively constant over a 20 min period and that MPIOs are rapidly cleared from the blood pool. This ensures high contrast, but is also a limitation in that the uptake of the CA is likely to be influenced by regional blood flow. The pattern of hypointensities observed with MRI was consistent with the distribution of [^{125}I]VCAM-MPIO as observed using phosphorimaging. Overall, this study provides proof of concept that multimodal imaging of inflammation with both SPECT and MRI is feasible. In the pilocarpine model of SE, MRI and SPECT/CT proved highly complementary, with inflammation detected in distinct brain regions by the two techniques, demonstrating the value of validating different imaging methods against one another.

MATERIALS AND METHODS

Synthesis of VCAM-MPIO. Monoclonal antibodies specific to rat VCAM-1 (MR106) (ebioscience, USA) were conjugated to micron-sized particles of iron oxide (MPIOs, 1 μm diameter, iron content: 26%, Invitrogen, Life Technologies, U.K.). In general, 40 μg of antibody was reacted per mg of iron/MPIO (Fe-MPIO) via a tosyl alkylation reaction following the manufacturers' guidelines and as previously reported. First, MPIOs were washed. The beads in the original vial were resuspended by vortexing for >30 s. The beads (5 mg of Fe per kg of animal weight, 19.2 mg/kg MPIO, 38 μL) were then placed in an eppendorf tube to which sodium borate buffer solution (1000 μL, 0.1 M, pH 9.5) was added and vortexed for >30 s. The eppendorf was placed next to a magnet (0.5 T, nickel plated, K&J Magnetics Inc., USA) to immobilize the particles, and the supernatant was removed with a Gilson pipette (Gilson Scientific Ltd., U.K.). After removing the tube from the magnet, to the washed beads was then added sodium borate solution (415 μL, 0.1 M, pH 9.5) followed by the antibodies (154 μg, 154 μL). Finally, ammonium sulfate solution (138 μL, 3 M dissolved in 0.1 M sodium borate buffer (100 mL, pH 9.4)) was added and the mixture was incubated overnight at 37 °C with slow shaking to ensure the beads did not settle during the incubation period. Following antibody conjugation, a magnet was used to immobilize VCAM-MPIO. The supernatant containing unbound antibodies was removed and VCAM-MPIO was resuspended in heparinized PBS (0.1%, 100 μL).

Synthesis of Iodine-125 Labeled VCAM-MPIO. [^{125}I]NaI (>12.95 GBq/ml, 629 GBq/mg) (PerkinElmer, USA) was purchased as a non-carrier-added solution in reductant free 10^{-5} M aqueous sodium hydroxide solution (pH 8−11). All other chemicals were purchased from Sigma-Aldrich U.K. unless otherwise stated.

VCAM-MPIO (19.2 mg MPIO, 40 μL) was suspended in heparinized phosphate-buffered saline (PBS) (100 μL, pH 7.4), and then transferred into precoated iodogen tubes (Thermo Fisher Scientific, USA). To this, [^{125}I]NaI (30−120 MBq) was added and the mixture was left to incubate at room temperature

DOI: 10.1021/acs.bioconjchem.5b00380
Bioconjugate Chem. 2015, 26, 1542−1549

for 30 min. After this time, the radioactive mixture was transferred into an eppendorf tube and radiolabeled VCAM-MPIO ([^{125}I]VCAM-MPIO) was purified using the magnetic immobilization technique described above. The particles were washed with PBS (1 mL) prior to their administration into rats. Using this same protocol, [^{125}I]IgG-MPIO was synthesized using nonspecific control antibodies (Southern Biotech, U.K).

Animal Models. All animal procedures were carried out in accordance with the UK Animals (Scientific Procedures) 1986 Act and institutional ethics regulations. Adult male Sprague–Dawley rats (170–270 g) were obtained from the breeding colony of the University College London (UCL) animal facility.

Neuroinflammation Model. Rats were anaesthetized using a combination of isoflurane (1% in pure oxygen) and urethane (1.5 g/kg, i.p.). TNF-α (300 ng, Life Technologies Ltd. U.K.) in saline (5 μL) was injected into the right striatum (coordinates from bregma: −0.5 mm anteroposterior, 3 mm mediolateral, 4 mm dorsoventral from dura) using a Hamilton syringe (Hamilton Company, USA) attached to a 31G needle. Saline (5 μL) was administered in place of TNF-α for the control group.

Lithium-Pilocarpine Model of Status Epilepticus (SE). Rats were injected with lithium chloride (3 mg/kg, intraperitoneally (i.p.)) 3 h prior to methyl scopolamine nitrate (5 mg/kg, i.p.) administration. This was followed 30 min later by administration of pilocarpine hydrochloride (30 mg/kg, i.p.) in order to induce SE (SE_{VCAM}). Animals were behaviorally assessed and the onset of SE was defined as stage 3 on the Racine scale. Diazepam (10 mg/kg, i.p., Hameln Pharmaceuticals, U.K.) was administered 90 min after SE onset to terminate the seizure. Further injections of diazepam were administered as required. The control groups received saline in place of pilocarpine hydrochloride.

Biological Evaluation of [^{125}I]VCAM-MPIO. Unless otherwise stated, rats were administrated [^{125}I]VCAM-MPIO or [^{125}I]IgG-MPIO (5 mg Fe/kg, 0.25–0.9 MBq/g) in heparinized phosphate-buffered saline (1 mL, pH 7.4) via a cannula inserted into the right external jugular vein.

Blood Clearance and Biodistribution. Blood samples (n = 3) were collected via a jugular vein cannula at predetermined time points (approximately: 85, 120 170, 230, 290 s) following radiolabeled MPIO administration in rats anaesthetized by a combination of isoflurane (1% in pure oxygen) and urethane (1.5 g/kg). After each collection, the cannula was flushed with saline (1 mL) to remove residual radioactivity. For biodistribution studies, radiolabeled MPIO (30–40 KBq/g) was administered via the lateral tail vein (n = 3). Ten minutes after tracer administration, the rats were anaesthetized with isoflurane in pure oxygen. Blood was sampled through cardiac puncture and the animals were sacrificed by cervical dislocation. The organs of interest were then removed for gamma counting (Wizard 2470, PerkinElmer, U.K.). The results are expressed as % injected dose per gram of tissue ± SD.

In Vivo Imaging. Inflammation was induced by intrastriatal injection of TNF-α as described above. Seven hours after the intracerebral injection (vide supra), [^{125}I]VCAM-MPIO or [^{125}I]IgG-MPIO was administered. Rats treated with Lithium-Pilocarpine received [^{125}I]VCAM-MPIO or [^{125}I]IgG-MPIO (SE_{VCAM} and SE_{IgG}) 20 h after the termination of seizures. For the sham control group saline was administered instead of pilocarpine ($SALINE_{VCAM}$). For the duration of the *in vivo* imaging experiments, isoflurane (1% in oxygen) was used to maintain anesthesia in rats. A physiological monitoring system (SA Instruments, USA) was used to monitor their respiration rate and rectal temperature. Temperature was maintained at 37 ± 0.5 °C using an air and water tubing warming system.

In vivo SPECT/CT (computed tomography) was performed using a nanoSPECT system (Bioscan Inc. USA) approximately 20 min post contrast administration. A CT scan was conducted with the following parameters: radial field of view (FOV) = 40.5 mm^2, axial FOV = 40.9 mm, exposure time per projection = 1 s, 360 projections, and 55 KvP tube voltage, which resulted in an acquisiton time of 6 min. Helical SPECT was performed across the same FOV using 2.5 mm pinhole apertures with 20 projections and an exposure time of 15 s per projection. For dynamic imaging, 5 scans were performed in succession resulting in a total imaging time of 25 min. All SPECT/CT images displayed are from the first frames captured 20 min post CA administration. To show the *in vivo* distribution of the CA, a scan was performed across the entire FOV of the animal with 2.5 mm pinhole apertures and an acquisition time of 40 min.

In vivo MRI was performed immediately following SPECT/CT imaging using a 9.4T horizontal bore scanner (Agilent Technologies, USA). MRI was performed between 1 and 2 h following administration of [^{125}I]VCAM-MPIO and [^{125}I]IgG-MPIO. Iron oxide was detected using a 3D gradient echo sequence (TR = 100 ms, TE = 11 ms, matrix = 192 × 192 × 160, FOV = 25 × 25 × 25 mm^3, acquisition time ≈ 51 min).

Phosphorimaging. Following *in vivo* imaging, the animals were euthanized, their brains were removed and fixed overnight in 4% paraformaldehyde (PFA) in PBS (pH 7.4). The brains were then cryoprotected overnight in sucrose solution and sectioned coronally at 20 μm. Sectioning of the brain commenced close to the bregma. The sections were then mounted on poly(L-lysine) coated glass slides (VWR international Ltd. U.K) which were subsequently exposed on unmounted GP 20 × 25 cm^2 phosphor screens (VWR international LTD, U.K.) for 15 min. After this time, the screens were scanned by a Typhoon 9410 Trio+ Phosphorimager (GE Healthcare, U.K.), (25 μm resolution, acquisition time = 2 h 30 min) and the resulting images were processed by ImageJ (NIH, USA).

As the radioactivity levels in the brain sections were above the optimal range for phosphorimaging, one animal in the TNF-α group was administered with a reduced dose of [^{125}I]VCAM-MPIO (3 mg Fe/kg, 30 kBq/g). The animal was sacrificed 1 h post CA administration, and the brain was removed and treated with PFA and sucrose as previously described. Coronal sections (20 μm) of the brain were exposed on a phosphor screen for 1 week, which was then scanned using the parameters described above.

Optical Imaging. In order to correlate the observed signals to particular brain regions, optical images of the sections used for phosphorimaging were captured on a bright field AxioSkop 2 system (Göttingen, Germany) at 5× magnification. The images were processed using the tiling and stitching method (Lundin M, 2004) on the Zeiss Axio Vision 4.8 software (Imaging Associates, Germany).

Image Analysis. *SPECT Reconstruction.* SPECT images were reconstructed using the HiSPECT software package using the following parameters: smoothing = 45%, resolution = 67%, number of iterations = 10. CT reconstruction was performed using InVivoScope (InviCRO, USA). For display purposes, the *in vivo* SPECT images are thresholded at 40% of the 95th percentile and linearly scaled between this value and the 95th percentile.

DOI: 10.1021/acs.bioconjchem.5b00380
Bioconjugate Chem. 2015, 26, 1542–1549

MRI Quantification of Contrast Agent Binding. MRI data were processed in MATLAB 2013a (MathWorks, Natick, MA). First, the data were zero-filled to 256 × 256 × 256 in *k*-space prior to reconstruction to give a final isotropic voxel size of 98 μm. Brain extraction was performed using a multiatlas approach.[26−28] Hypointensities caused by the presence of iron oxide were segmented using adaptive thresholding in order to take into account local variations in signal intensity. This was achieved by subtracting the MRI volume from the volume convolved with a three-dimensional Gaussian kernel of size 15 × 15 × 15 voxels and a σ of 15, followed by thresholding with the same empirically determined threshold used across all data sets. Regions of interest (ROIs) were defined over the left or right cerebral hemisphere surrounding the injection site. These consisted of 30 consecutive slices (~3 mm) anterior to and 30 consecutive slices posterior to the injection site (as indicated in Figure 4a and b).

Coregistration. Coregistration of MRI and CT images was performed in AMIRA (Visualization Sciences Group, Burlington, MA) on the gradient images of the brain extracted MRI magnitude data and the CT intensity images using normalized correlation as the cost function.

SPECT Quantification of Contrast Agent Binding. ROIs as defined on MRI images were propagated to the SPECT/CT native space using the same transformation matrix. In this way, identical ROIs were used for both the MRI and SPECT analyses. Background signal intensity was defined as the mean signal intensity across all nonbrain tissue across the entire 3D field of view and CA binding was expressed as the signal-to-background ratio to normalize counts for body weight and the level of radioactivity that was administered.

Statistical Analysis. Statistical analysis was performed in MATLAB. Group means were compared using one-way ANOVA. Group means between the left and right hemispheres were compared using one-tailed paired *t* tests. All error bars are shown as mean ± standard error of the mean (SEM). Statistical significance was assigned at $p < 0.05$.

■ ASSOCIATED CONTENT

Supporting Information

The Supporting Information is available free of charge on the ACS Publications website at DOI: 10.1021/acs.bioconjchem.5b00380.

Ex vivo biodistribution ^{125}I labeled VCAM-MPIO in healthy rats; dynamic SPECT following administration of the CA in TNF-α treated rats; MRI images showing the distribution of VCAM-MPIO (PDF)

■ AUTHOR INFORMATION

Corresponding Author

*E-mail: e.arstad@ucl.ac.uk.

Author Contributions

#N. Patel and B. A. Duffy contributed equally.

Notes

The authors declare no competing financial interest.

■ ACKNOWLEDGMENTS

This work was funded by the UK Medical Research Council, (B.D., N.P.) and was undertaken at UCLH/UCL who received a proportion of funding from the Department of Health's NIHR Biomedical Research Centres funding scheme (E.A.). The research leading to these results has received funding from the European Union's Seventh Framework Programme (FP7/2007-2013) under grant agreement n°602102 (EPITARGET) (E.A.). We also acknowledge support from King's College London and UCL Comprehensive Cancer Imaging Centre CR-UK & EPSRC, in association with the MRC and DoH (England) (M.L.) M.L. receives funding from Medical Research Council (MR/J013110/1); the National Centre for the Replacement, Reduction and Refinement of Animal in Research (NC3Rs); UK Regenerative Medicine Platform Safety Hub (MRC: MR/K026739/1).

■ REFERENCES

(1) del Zoppo, G., Ginis, I., Hallenbeck, J. M., Iadecola, C., Wang, X., and Feuerstein, G. Z. (2000) Inflammation and stroke: putative role for cytokines, adhesion molecules and iNOS in brain response to ischemia. *Brain Pathol. 10*, 95−112.

(2) Vezzani, A., and Granata, T. (2005) Brain inflammation in epilepsy: Experimental and clinical evidence. *Epilepsia 46*, 1724−1739.

(3) Morganti-Kossmann, M. C., Rancan, M., Stahel, P. F., and Kossmann, T. (2002) Inflammatory response in acute traumatic brain injury: a double-edged sword. *Curr. Opin. Crit. Care. 8*, 101−105.

(4) Serres, S., Soto, M. S., Hamilton, A., McAteer, M. A., Carbonell, W. S., Robson, M. D., Ansorge, O., Khrapitchev, A., Bristow, C., Balathasan, L., et al. (2012) Molecular MRI enables early and sensitive detection of brain metastases. *Proc. Natl. Acad. Sci. U. S. A. 109*, 6674−6679.

(5) Soto, M. S., Serres, S., Anthony, D. C., and Sibson, N. R. (2014) Functional role of endothelial adhesion molecules in the early stages of brain metastasis. *Neuro Oncol. 16*, 540−551.

(6) Tuppo, E. E., and Arias, H. R. (2005) The role of inflammation in Alzheimer's disease. *Int. J. Biochem. Cell Biol. 37*, 289−305.

(7) McAteer, M. A., Sibson, N. R., von zur Muhlen, C., Schneider, J. E., Lowe, A. S., Warrick, N., Channon, K. M., Anthony, D. C., and Choudhury, R. P. (2007) In vivo magnetic resonance imaging of acute brain inflammation using microparticles of iron oxide. *Nat. Med. 13*, 1253−1258.

(8) Hoyte, L. C., Brooks, K. J., Nagel, S., Akhtar, A., Chen, R. L., Mardiguian, S., McAteer, M. A., Anthony, D. C., Choudhury, R. P., Buchan, A. M., et al. (2010) Molecular magnetic resonance imaging of acute vascular cell adhesion molecule-1 expression in a mouse model of cerebral ischemia. *J. Cereb. Blood Flow Metab. 30*, 1178−1187.

(9) Serres, S., Mardiguian, S., Campbell, S. J., McAteer, M. A., Akhtar, A., Krapitchev, A., Choudhury, R. P., Anthony, D. C., and Sibson, N. R. (2011) VCAM-1-targeted magnetic resonance imaging reveals subclinical disease in a mouse model of multiple sclerosis. *FASEB J. 25*, 4415−4522.

(10) Duffy, B. A., Choy, M., Riegler, J., Wells, J. A., Anthony, D. C., Scott, R. C., and Lythgoe, M. F. (2012) Imaging seizure-induced inflammation using an antibody targeted iron oxide contrast agent. *NeuroImage 60*, 1149−1155.

(11) Montagne, A., Gauberti, M., Macrez, R., Jullienne, A., Briens, A., Raynaud, J.-S., Louin, G., Buisson, A., Haelewyn, B., Docagne, F., et al. (2012) Ultra-sensitive molecular MRI of cerebrovascular cell activation enables early detection of chronic central nervous system disorders. *NeuroImage 63*, 760−770.

(12) Akhtar, A. M., Chen, Y., Schneider, J. E., Digby, J. E., McAteer, M. A., Wood, K., and Choudhury, R. P. (2008) Magnetic Resonance Imaging Of Renal Ischemia Reperfusion Injury Using Microparticles Of Iron Oxide Targeting VCAM-1. *Circulation 118*, S_555.

(13) McAteer, M. A., Schneider, J. E., Ali, Z. A., Warrick, N., Bursill, C. A., von zur Muhlen, C., Greaves, D. R., Neubauer, S., Channon, K. M., and Choudhury, R. P. (2007) Magnetic resonance imaging of endothelial adhesion molecules in mouse atherosclerosis using dual-targeted microparticles of iron oxide. *Arterioscler., Thromb., Vasc. Biol. 28*, 77−83.

(14) Akhtar, A. M., Schneider, J. E., Chapman, S. J., Jefferson, A., Digby, J. E., Mankia, K., Chen, Y., McAteer, M. A., Wood, K. J., and Choudhury, R. P. (2010) In vivo quantification of VCAM-1 expression

in renal ischemia reperfusion injury using non-invasive magnetic resonance molecular imaging. *PLoS One 5*, e12800−e.
(15) Elices, M. J., Osborn, L., Takada, Y., Crouse, C., Luhowskyj, S., Hemler, M. E., and Lobb, R. R. (1990) VCAM-1 on Activated Endothelium Interacts with the Leukocyte Integrin VLA-4 at a Site Distinct from the VLA-4 Fibronectin Binding-Site. *Cell 60*, 577−584.
(16) Fabene, P. F., Mora, G. N., Martinello, M., Rossi, B., Merigo, F., Ottoboni, L., Bach, S., Angiari, S., Benati, D., Chakir, A., et al. (2008) A role for leukocyte-endothelial adhesion mechanisms in epilepsy. *Nat. Med. 14*, 1377−1383.
(17) Shapiro, E. M., Skrtic, S., and Koretsky, A. P. (2005) Sizing it up: Cellular MRI using micron-sized iron oxide particles. *Magn. Reson. Med. 53*, 329−338.
(18) Louie, A. (2010) MultimodalityImaging Probes: Design and Challenges. *Chem. Rev. 110*, 3146−3195.
(19) Xie, J., Liu, G., Eden, H. S., Al, H., and Chen, X. (2011) Surface-engineered magnetic nanoparticle platforms for cancer imaging and therapy. *Acc. Chem. Res. 44*, 883−892.
(20) Sun, X., Cai, W., and Chen, X. (2015) Positron Emission Topography Imaging Using Radiolabeled Inorganic Nanomaterials. *Acc. Chem. Res. 48*, 286−294.
(21) Tamba, B. I., Dondas, A., Leon, M., Neagu, A. N., Dodi, G., Stefanescu, C., and Tijani, A. (2015) Silica Nanoparticles: Prerparation, Characterization, and *In Vitro/In Vivo* Biodistribution Studies. *Eur. J. Pharm. Sci. 71*, 46−55.
(22) Scremin, O. U. (2004) Cerebral Vascular System. *The Rat Nervous System*, 3rd ed. (Paxinos, G.) pp 1167−1202, Chapter 33, Academic Press, Burlington.
(23) Muro, S., Garnacho, C., Champion, J. A., Leferovich, J., Gajewski, C., Schuchman, E. H., Mitragotri, S., and Muzykantov, V. R. (2008) Control of Endothelial Targeting and Intracellular Delivery of Therapeutic Enzymes by Modulating the Size and Shape of ICAM-1 targeted Carriers. *Mol. Ther. 16*, 1450−1458.
(24) Benezra, M., Penate-Medina, O., Zanzonico, P. B., Schaer, D., Ow, H., Burns, A., DeStanchina, E., Longo, V., Herz, E., Iyer, S., et al. (2011) Multimodal Silica Nanoparticles are Effectiver Cancer-Targeted Probes in a Model of Human Melanoma. *J. Clin. Invest. 121*, 2768−2780.
(25) Mendonca Dias, M. H., and Lauterbur, P. C. (1987) Contrast agents for magnetic resonance imaging. *Biol. Trace Elem. Res. 13*, 229−239.
(26) Duffy, B. A., Chun, K. P., Ma, D., Lythgoe, M. F., and Scott, R. C. (2014) Dexamethasone exacerbates cerebral edema and brain injury following lithium-pilocarpine induced status epilepticus. *Neurobiol. Dis. 63*, 229−36.
(27) Ma, D., Cardoso, M. J., Modat, M., Powell, N., Wells, J., Holmes, H., Wiseman, S., Tybulewicz, V., Fisher, E., Lythgoe, M. F., et al. (2014) Automatic structural parcellation of mouse brain MRI using multi-atlas label fusion. *PLoS One 9*, e86576.
(28) Jenks, K. R., Lucas, M. M., Duffy, B. A., Robbins, A. A., Gimi, B., Barry, J. M., and Scott, R. C. (2013) Enrichment and training improve cognition in rats with cortical malformations. *PLoS One 8*, e84492.

DOI: 10.1021/acs.bioconjchem.5b00380
Bioconjugate Chem. 2015, 26, 1542−1549